ELSEVIER

Chemical Physics 183 (1994) 217–233

Chemical Physics

Solvation dynamics of LDS 750 in associative liquids by degenerate four-wave mixing and time-resolved emission techniques

S.Y. Goldberg, E. Bart, A. Meltsin, B.D. Fainberg, D. Huppert

Raymond and Beverly Sackler Faculty of Exact Sciences, School of Chemistry, Tel-Aviv University, Tel-Aviv 69978, Israel

Received 15 July 1993; in final form 20 January 1994

Abstract

We developed theoretically and experimentally the principles of a spectroscopical method based on resonance transient population gratings for a quantitative description of solvation dynamics of large molecules in liquid solutions. The solvation dynamics of LDS 750 in methanol, 1,2-ethanediol, 1,3-propanediol and 1,4-butanediol have been measured over four time decades from 100 fs to 1000 ps. The solvation dynamics of LDS 750 in all solvents consists of ultrafast as well as slow components.

1. Introduction

The dynamics of solvation has been extensively studied [1–5] both experimentally [6–15] and theoretically [16–25] in the last decade. Most of the experimental effort in solvation dynamics is based on measurements of emission time-dependent Stokes shift of probe molecules dissolved in polar solvents. Picosecond [1,2] and later on subpicosecond [12] time-resolved fluorescence spectroscopy provided important information on the microscopic solvation dynamics in polar liquids. The experimental effort was further supplemented by results of molecular dynamics simulations of model polar liquids [28–32]. In early experimental and theoretical studies the solvation dynamics results were related to the solvent orientational motion. The first results [1,2] were described by the continuum model predicting a uniform exponential solvation dynamics for Debye solvents with solvation times given by the longitudinal relaxation time given by $\tau_L = (\varepsilon_\infty/\varepsilon_S)\tau_D$, where τ_D is the dielectric relaxation time and ε_S and ε_∞ are the static and the high frequency dielectric constants, respectively. The model implies that the solvent dynamics is independent of the distance from the photoexcited probe molecule. Careful examination of the experimental results has shown that the solvation dynamics is nonexponential even in nonassociated solvents while in the macroscopic dielectric relaxation measurements of such solvents a single exponential relaxation was observed. Rips, Klafter and Jortner [19,20] explained the nonexponential behavior of solvation dynamics by extending the mean spherical approximation (MSA) to the dynamic region. Onsager [21] proposed the "inverted snow ball" model where the solvation proceeds from the "outside to the inside". Far from the photo-excited probe molecule the solvation time is τ_L, while in the close vicinity of the probe, the relaxation is slower and decreases to τ_D. This prediction has been derived quantitatively by Rips et al. [20]. Simulations of solvation dynamics [28–32] have shown that the fastest solvation process occurs at the first solvation shell and thus in contrast to the "inverse

SSDI 0301-0104 (94)00097-T

snowball'' model. Recent ultrafast time-dependent Stokes shift measurements of LDS 750 in acetonitrile [12] and nonresonant optical Kerr effect measurements of acetonitrile [13] with 50–100 fs laser pulses have shown that the early stage of solvation dynamics is ultrashort ~70 fs and has a Gaussian shape. The Gaussian decay found in the ultrafast solvation experiments has been known previously from far-infrared spectroscopy [33,34] as well as molecular dynamics simulations and the Anderson–Kubo stochastic modulation theory [19,35]. The Gaussian component is attributed to the inertial solvent motion. The inertial part accounts for ~80% of the total solvation energy in acetonitrile. The inertial solvation dynamics of LDS 750 in acetonitrile [12] is followed by an exponential decay with ~200 fs decay time.

In this study we propose a spectroscopical method for the observation of ultrafast solvation dynamics: the resonance transient population grating spectroscopy (RTPGS) [36–42]. This method is characterized by high sensitivity and high time resolution limited by the laser pulse width.

The RTPGS method is applied to study the solvation dynamics of LDS 750 in highly viscous associative protic solvents such as diols. The diols are highly viscous at room temperature but their orientational longitudinal relaxation times are comparable to the monoalcohols while the monoalcohol viscosities are approximately ten times smaller [14].

We shall show theoretically and experimentally that the RTPGS is rather sensitive to solvation dynamics and reflects its fine details.

2. Theoretical background

Consider a molecule with two electronic states $n=1$ and 2 in a solvent described by the Hamiltonian

$$H_0 = \sum_{n=1}^{2} |n\rangle [E_n - i\hbar\gamma_n + W_n(\boldsymbol{Q})] \langle n| ,$$

$$E_2 > E_1 , \qquad (1)$$

where E_n and $2\gamma_n$ are the energy and inverse lifetime of state n, $W_n(\boldsymbol{Q})$ is the adiabatic Hamiltonian of a reservoir (the vibrational subsystems of a molecule and a solvent interacting with the two-level electron system under consideration in state n). The molecule is affected by electromagnetic radiation,

$$\boldsymbol{E}(\boldsymbol{r}, t) = \boldsymbol{E}^{+}(\boldsymbol{r}, t) + \boldsymbol{E}^{-}(\boldsymbol{r}, t)$$

$$= \tfrac{1}{2} \sum_{m=1}^{3} \{\boldsymbol{e}_m \mathscr{E}_m(t) \exp[i(\boldsymbol{k}_m \cdot \boldsymbol{r} - \omega t) + \text{c.c.}]\} .$$

Here $\boldsymbol{E}^{+(-)}$ are the positive (negative) frequency components of the field strength, ω is the field frequency; $\boldsymbol{e}_m$, $\mathscr{E}_m(t)$ and $\boldsymbol{k}_m$ are the polarization vector, the strength amplitude and wave vector of the mth field.

Since we are interested in intermolecular relaxation processes, we shall single out the solvent contributions to E_n and $W_n(\boldsymbol{Q})$,

$$E_n = E_n^0 + \langle V_n^{el} \rangle , \qquad (2)$$

$$W_n(\boldsymbol{Q}) = W_{n\mathrm{M}} + W_{\mathrm{S0}} + W_{n\mathrm{S}} , \qquad (3)$$

where W_{S0} is the Hamiltonian governing the nuclear degrees of freedom of the solvent in the absence of the solute, $W_{n\mathrm{M}}$ is the Hamiltonian representing the nuclear degrees of freedom of a solute molecule, E_n^0 is the energy of state n of the isolated molecule, $W_{n\mathrm{S}}$ and V_n^{el} describe interactions between the solute and the nuclear and electronic degrees of freedom of the solvent, respectively. It is possible to replace the operators V_n^{el} in the Hamiltonian by their expectation values $\langle V_n^{el} \rangle$ [43].

In transient four-photon spectroscopy two pump pulses with wave vectors $\boldsymbol{k}_1$ and $\boldsymbol{k}_2$ create a light-induced grating in the sample under investigation with a wave vector $\boldsymbol{q}_1 = \boldsymbol{k}_1 - \boldsymbol{k}_2$ (see Fig. 4 below). The grating effectiveness is measured by the diffraction of a time-delayed probe pulse $\boldsymbol{k}_3$ with the generation of a signal with a new wave vector $\boldsymbol{k}_{\mathrm{S}} = \boldsymbol{k}_3 + (\boldsymbol{k}_1 - \boldsymbol{k}_2)$. The signal intensity J_{S} can be calculated from the positive frequency component of the cubic polarization:

$$J_{\mathrm{S}}(\tau) \sim \int_{-\infty}^{\infty} \mathrm{d}t \, |\boldsymbol{P}^{(3)+}(\boldsymbol{r}, t)|^2 , \qquad (4)$$

where τ is the delay time of the probe pulse $\boldsymbol{k}_3$ with respect to the pump ones. We shall calculate $\boldsymbol{P}^{(3)+}(\boldsymbol{r}, t)$, using a general theory [40,44–46]:

$$\boldsymbol{P}^{(3)+}(\boldsymbol{r}, t) = \sum_{mm'm''} \boldsymbol{B}_{mm'm''} \int_0^\infty\int_0^\infty\int_0^\infty \mathrm{d}\tau_1\, \mathrm{d}\tau_2\, \mathrm{d}\tau_3$$
$$\times \exp\{-[\mathrm{i}(\omega_{21}-\omega)+\gamma]\tau_1 - \tau_2/T_1\}$$
$$\times \mathscr{E}_{m''}(t-\tau_1)\{\mathscr{E}_{m'}(t-\tau_1-\tau_2)$$
$$\times \mathscr{E}^*_{m}(t-\tau_1-\tau_2-\tau_3)$$
$$\times \exp\{[\mathrm{i}(\omega_{21}-\omega)-\gamma]\tau_3\} F_1(\tau_1, \tau_2, \tau_3)$$
$$+ \mathscr{E}_{m'}(t-\tau_1-\tau_2-\tau_3)\mathscr{E}^*_{m}(t_1-\tau_1-\tau_2)$$
$$\times \exp\{-[\mathrm{i}(\omega_{21}-\omega)+\gamma]\tau_3\} F_2(\tau_1, \tau_2, \tau_3)\}, \quad (5)$$

where

$$\boldsymbol{B}_{mm'm''} = \frac{-\mathrm{i}NL^4}{8\hbar^3} |D^{\mathrm{el}}_{12}|^4$$
$$\times \langle \boldsymbol{\kappa}^*(\boldsymbol{\kappa}\cdot\boldsymbol{e}_{m''})(\boldsymbol{k}\cdot\boldsymbol{e}_{m'})\rangle_{\mathrm{or}}$$
$$\times \exp\{\mathrm{i}[(\boldsymbol{k}_{m'} + \boldsymbol{k}_{m''} - \boldsymbol{k}_m)\cdot\boldsymbol{r} - \omega t]\},$$

$\boldsymbol{\kappa} D^{\mathrm{el}}_{12}$ is a matrix element of the dipole-moment operator taken with respect to the electron wave function; $\langle\ldots\rangle_{\mathrm{or}}$ signifies averaging over various molecule orientations, $T_1 = (2\gamma_2)^{-1} \equiv (2\gamma)^{-1}$ is the lifetime of the excited state 2; $\omega_{21} = (E^0_2 + \langle V^{\mathrm{el}}_2\rangle - E^0_1 - \langle V^{\mathrm{el}}_1\rangle)/\hbar + \langle W_2 - W_1\rangle/\hbar$ is the frequency of the $1 \rightarrow 2$ Franck–Condon transition. The angle brackets indicate thermal averaging over the variables of the vibrational subsystems in the ground electronic state of the molecule, N is the system particle density and L is the Lorentz correction factor for a local field. The summation in Eq. (5) is carried out over all fields that satisfy the condition $\boldsymbol{k}_{\mathrm{S}} = \boldsymbol{k}_{m'} + \boldsymbol{k}_{m''} - \boldsymbol{k}_m$.

The functions $F_{1,2}(\tau_1, \tau_2, \tau_3)$ are sums of four-time correlation functions [40,44–47], corresponding to the four-photon character of interaction:

$$F_1(\tau_1, \tau_2, \tau_3) = K(0, \tau_3, \tau_1+\tau_2+\tau_3, \tau_2+\tau_3) + K(0, \tau_2+\tau_3, \tau_1+\tau_2+\tau_3, \tau_3), \quad (6a)$$

$$F_2(\tau_1, \tau_2, \tau_3) = K^*(0, \tau_3, \tau_2+\tau_3, \tau_1+\tau_2+\tau_3) + K^*(0, \tau_1+\tau_2+\tau_3, \tau_2+\tau_3, \tau_3), \quad (6b)$$

$$K(0, t_1, t_2, t_3) = \langle \exp(\mathrm{i}\hbar^{-1}\tilde{W}_2 t_1) \exp[\mathrm{i}\hbar^{-1}W_1(t_2-t_1)] \times \exp[-\mathrm{i}\hbar^{-1}\tilde{W}_2(t_2-t_3)] \exp(-\mathrm{i}\hbar^{-1}\tilde{W}_2 t_3)\rangle . \quad (7)$$

The value $u = W_2 - W_1 - \langle W_2 - W_1\rangle \equiv \tilde{W}_2 - W_1$ represents both perturbations of the molecular nuclear system and the solvent nuclear system respectively during the electronic transition. We can divide the operator u into the intra (M) and inter (S) molecular contributions, $u = u_{\mathrm{M}} + u_{\mathrm{S}}$, where $u_{\mathrm{M,S}} = W_{2\mathrm{M,S}} - W_{1\mathrm{M,S}} - \langle W_{2\mathrm{M,S}} - W_{1\mathrm{M,S}}\rangle$.

$$u(t) = \exp(\mathrm{i}\hbar^{-1}W_1 t)u(Q)\exp(\mathrm{i}\hbar^{-1}W_1 t)$$

It is apparent that the values $K(0, t_1, t_2, t_3)$ (Eq. (7)) can be represented in the form

$$K(0, t_1, t_2, t_3) = K_{\mathrm{M}}(0, t_1, t_2, t_3)K_{\mathrm{S}}(0, t_1, t_2, t_3) \quad (8)$$

due to the fact that $u = u_{\mathrm{M}} + u_{\mathrm{S}}$.

It is very important for the following discussion to determine exactly the processes which we want to investigate. We intend to study the solvation dynamics processes by degenerate four-wave mixing, and by time-resolved luminescence (TRL), which has been used in most of the solvation studies in the past [6–14]. The hot luminescence processes occur after the completion of the electronic transition phase relaxation, during the vibrational relaxation in the excited electronic state. Therefore, we have to conduct our resonance four-photon wave mixing experiment by such a way to avoid the polarization gratings and to preserve the population gratings. The polarization gratings are destroyed during the phase relaxation time T' of the electronic transition, and the population ones are destroyed during the vibrational relaxation time τ_{c}.

We shall consider molecules with broad structureless (or weakly structured) electronic spectra for which the following inequality is fulfilled:

$$\sigma_2 \tau_{\mathrm{c}}^2 \gg 1,$$

where σ_2 is the second central moment of an electronic spectrum. It has been demonstrated that the following times are typical for the time evolution of the system investigated [40,42,48]:

$$\sigma_2^{-1/2} < T' \ll \tau_{\mathrm{c}},$$

where $\sigma_2^{-1/2}$ plays the role of the reversible dephasing time of an electronic transition, $T' = (\tau_c \sigma_2^{-1})^{1/3}$ plays the role of the irreversible dephasing time, and τ_c plays the role of the relaxation time of populations. The typical value of the irreversible dephasing time for complex molecules in solutions for usual conditions $T' \approx 25$ fs [40]. Therefore, the character of the response of the system under study ($\sigma_2 \tau_c^2 \gg 1$) in degenerate four-wave mixing experiment (Fig. 4) depends on the relation between T' and the pump pulses duration t_p [40,42].

The pump pulses $\boldsymbol{k}_1$ and $\boldsymbol{k}_2$ form a polarization and a population grating. The polarization grating decays with a characteristic time constant $\sim T'$. Therefore, if the pulse duration $t_p \gg T' > \sigma_2^{-1/2}$ (and naturally, $\tau \sim t_p \gg T'$), only the population grating preserves and the probing pulse $\boldsymbol{k}_3$, delayed by time τ, allows one to measure the population grating relaxation [40,42].

Thus, a four-wave mixing experiment will provide similar (but not identical) information as TRL experiments (solvation dynamics), if relatively long pump pulses $t_p \gg T'$ will be used.

In our experiment the pump pulse duration $t_p \gg T'$ ($t_p \sim 150$ fs). It is worth noting that resonance degenerate four-wave mixing experiments with very short pump pulses $t_p \sim 10$ fs have been conducted in several studies [15,49,50]. Since in these experiments $t_p < T'$, the signal must be different from our experiments as indicated in the former theoretical calculations [40,42]. The following simple arguments show the difference in signal behaviors in degenerate four-wave mixing experiments with $t_p \sim 10\,\text{fs} \lesssim \sigma_2^{-1/2} < T'$ and $t_p \gg T' > \sigma_2^{-1/2}$, correspondingly. Relatively long pump pulses $t_p \gg T'$ of frequency ω create a hole in the initial thermal distribution relative to a generalized solvation coordinates in the ground electronic state (Fig. 1a) and, simultaneously, a narrow spike in the excited electronic state. These changes are measured by the probe pulse at the same frequency ω.

In the case of very short pulses $t_p < \sigma_2^{-1/2} < T'$ in the framework of the picture shown in Fig. 1a (vertical optical transitions), the spectral width of such pulses $\Delta\omega \sim 1/t_p$ is sufficient to excite the whole ground state distribution and for the creation of a very broad spike in the excited state. The absorption energy of a very short probe pulse can be of very little sensitivity to the relaxation of the created broad spike in the excited state, especially in the case of $t_p \ll \sigma_2^{-1/2}$. Such a situation is opposite to the case with long pulses $t_p \gg T' > \sigma_2^{-1/2}$.

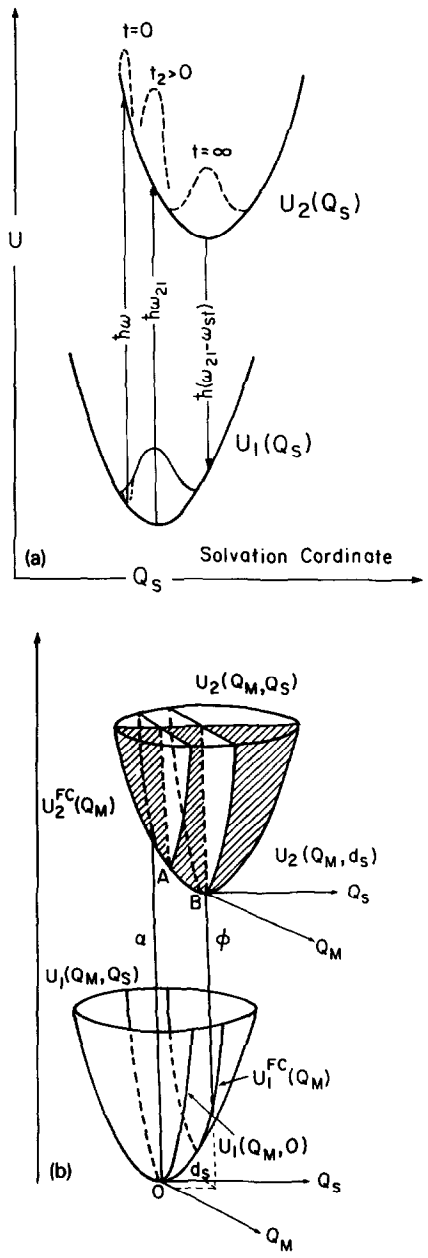

Fig. 1. Potential surfaces of the ground and the excited electronic states of a solute molecule in liquid. (a) One-dimensional potential surfaces as a function of a generalized solvent polarization coordinate. (b) Two-dimensional potential surfaces of the ground and the excited electronic states.

We do not deliberately draw the picture corresponding to excitation by very short pulses, because for them ($t_p \ll T'$) the picture of vertical transitions (Fig. 1) is incorrect [40,42,48]. Such pulses ($t_p \ll T'$) excite coherent effects (polarization grating) and, as a matter of fact, degenerate four-wave mixing with pulses $t_p \ll T'$ represents the case of stimulated photon echo spectroscopy [15]. In this section we only wanted to emphasize the difference between degenerate four-waving mixing spectroscopy using short pulse durations $t_p < T'$ and long one $t_p \gg T'$. In the next sections we shall term degenerate four-wave mixing spectroscopy with long pump pulses $t_p \gg T'$ as resonant transient population grating spectroscopy (RTPGS).

We shall use some assumptions on calculating the cubic polarization $\boldsymbol{P}^{(3)+}(\boldsymbol{r}, t)$ from the general equations (5)–(7).

(1) We shall use a Gaussian approximation for the value u_S representing the perturbation of the solvent nuclear system during the electronic transition. The Gaussian approximation is valid for the description of the intermolecular relaxation [43,51]. The interaction energy of the solute molecule with its surroundings can be represented as the sum of the energy of interaction with the individual solvent molecules. Accordingly, the quantity $u_S(t)$ can be also represented as a sum $u_S(t) = \sum_j u_{Sj}(t)$ of random variables $u_{Sj}(t)$ associated with the jth solvent molecule, correspondingly. The number of such solvent molecules (j) can be quite large (in the absence of specific chemical interactions). In addition the contributions $u_{Sj}(t)$ can be considered for a liquid as weakly correlated. According to the central limit theorem of the probability theory [52], these properties of $u_{Sj}(t)$ permit one to consider the magnitude $u_S(t)$ as a Gaussian stochastic function [51].

In this case the four-time correlation function $K_S(0, t_1, t_2, t_3)$ (Eqs. (7),(8)) can be represented as follows [40,44–46];

$$K_S(0, t_1, t_2, t_3) = \exp[g_S(t_3 - t_2) + g_S(t_1) + g_S(t_2 - t_1) - g_S(t_2) - g_S(t_3 - t_1) + g_S(t_3)], \quad (9)$$

where

$$g_S(t) = -\hbar^{-2} \int_0^t dt' \, (t - t') \langle u_S(0) u_S(t') \rangle ,$$

$$\langle u_S(0) u_S(t) \rangle \equiv \hbar^2 \sigma_{2S} S(t) . \quad (10)$$

$S(t)$ is the solute–solvent correlation function, $\sigma_{2S} = \langle u_S^2(0) \rangle \hbar^{-2}$ is the contribution of the solvent to the second central moment of both the absorption and the luminescence spectra.

We shall consider the translational and the rotational motions of the liquid molecules as classical, at room temperature, since their characteristic frequencies are smaller than the thermal energy kT. The solvent contribution ω_{St} to the Stokes shift of the equilibrium spectra of the absorption as well as the emission is of the order of $1000\,cm^{-1}$. For the classical case we have [43,51,53]

$$\sigma_{2S} = \omega_{St} kT/\hbar . \quad (11)$$

Let us denote by τ_S the characteristic decay time of the "intermolecular" correlation function $\langle u_S(0) u_S(t) \rangle$. In any case $\tau_S \gtrsim 10^{-13}$ s [13]. Since $\sigma_{2S}^{-1/2} \sim 10^{14}$ s, the parameter $\sigma_{2S} \tau_S^2 \gtrsim 10^2 \gg 1$. For this case we can write [40,44–46]

$$K_S(0, \tau_3, \tau_1 + \tau_2 + \tau_3, \tau_2 + \tau_3) = \exp\{-\tfrac{1}{2}\sigma_{2S}[\tau_1^2 + \tau_3^2 - 2\tau_1 \tau_3 S(\tau_2)]\} , \quad (12a)$$

$$K_S^*(0, \tau_3, \tau_2 + \tau_3, \tau_1 + \tau_2 + \tau_3) = \exp\{-\tfrac{1}{2}\sigma_{2S}[\tau_1^2 + \tau_3^2 + 2\tau_1 \tau_3 S(\tau_2)]\} , \quad (12b)$$

$$K_S(0, \tau_2 + \tau_3, \tau_1 + \tau_2 + \tau_3, \tau_3) = \exp\{i\omega_{St}[1 - S(\tau_2)]\} \times K_S(0, \tau_3, \tau_1 + \tau_2 + \tau_3, \tau_2 + \tau_3) , \quad (13a)$$

$$K_S^*(0, \tau_1 + \tau_2 + \tau_3, \tau_2 + \tau_3, \tau_3) = \exp\{i\omega_{St}[1 - S(\tau_2)]\} \times K_S^*(0, \tau_3, \tau_2 + \tau_3, \tau_1 + \tau_2 + \tau_3) . \quad (13b)$$

(2) For simplicity, we shall also use a Gaussian approximation for the quantity u_M representing the perturbation of the molecular nuclear system during an electronic transition. Such an approximation is correct for harmonic molecular vibrations in the case of a linear electronic vibrational coupling, and hence the absorption and emission spectra reduces to mirror symmetrical spectra.

In a Gaussian approximation the four-photon correlation functions $K_M(0, t_1, t_2, t_3)$ (Eqs. (7), (8)) are also determined by Eq. (9) where one has to replace the quantities $g_S(t)$ and $\langle u_S(0) u_S(t) \rangle$ by $g_M(t)$ and $\langle u_M(0) u_M(t) \rangle$, correspondingly. It is worthwhile to

note that Eq. (9) is also correct in the case of the non-Gaussian contribution to the quantity u. However, such contributions must be small. Non-Gaussian contributions to u_M can be determined by the quadratic electronic vibrational interaction and anharmonicity. However, for the $S_0 \rightarrow S_1$ optical transition in large molecules, such effects are usually small in comparison with the linear electronic vibrational coupling and therefore in many cases perturbation theory is sufficient to calculate their contributions.

The assumption that u_M is Gaussian is not obligatory. The generalization for the case of an arbitrary nature of u_M will be published elsewhere.

(3) Numerous experiments [54–56] show that the Franck–Condon molecular state, achieved by an optical excitation, relaxes very fast, and the intramolecular spectra spectrum forms within 0.1 ps. Therefore, we shall consider that in our experiments, the intramolecular relaxation takes place within the pulse duration ($t_p \approx 150$ ps) [#1]. More exactly, there are a fast and a slow steps in the relaxation of a Franck–Condon state. The faster component is mainly determined by the intramolecular relaxation while the slower step is determined by the intermolecular relaxation. This assumption is not critical for the theory. It is necessary only for carrying out specific calculations.

It follows from Eqs. (12) and (13) that the intermolecular relaxation is described by the correlation function $S(\tau_2)$, and the upper boundary values for the times τ_1 and $\tau_3 \sim \sigma_{2S}^{-1/2}$. Therefore, we can equate $\tau_1 \approx \tau_3 \approx 0$ in the arguments of the field functions $\mathscr{E}_m$, $\mathscr{E}_{m'}$, $\mathscr{E}_{m''}$ in Eq. (5) [39,40,57]. In addition, the time τ_2 is of the order of the intermolecular relaxation time τ_S. The intramolecular functions $g_M(t)$, which depend on τ_2, will attenuate to zero in accordance with the assumption that the intramolecular relaxation is faster than the intermolecular one. Keeping this in mind, we can write the quantities F_1 and F_2 (Eqs. (6)) in the form, using Eqs. (12) and (13):

$$F_{1,2} = \{\exp[g_M(-\tau_1)] + \exp\{g_M(\tau_1) + i\omega_{St}[1 - S(\tau_2)]\} \times \exp\{-\tfrac{1}{2}\sigma_{2S}[\tau_1^2 + \tau_3^2 \mp 2\tau_1\tau_3 S(\tau_2)] + g_M(\pm\tau_3)\}, \quad (14)$$

where

$$g_M(t) = -\hbar^{-2} \int_0^t dt' \, (t - t')\langle u_M(0) u_M(t')\rangle$$

is the logarithm of the characteristic function (Fourier transformation) of the "intramolecular" spectrum of one-photon absorption after subtraction of a term which determines the first moment of the spectrum.

We can integrate the right-hand side of Eq. (5) with respect to τ_1 and τ_3, using (14) and the approximate independence of the fields $\mathscr{E}_m$ on these time arguments. Using Eqs. (4), (5), and (14), we obtain for the signal excited by nonoverlapping pulses which are short with respect to the intermolecular relaxation time

$$J_S(\tau) \sim \exp(-2\tau/T_1) \; |A(\tau)|^2 . \quad (15)$$

The term $\exp(-\tau/T_1)$ describes the attenuation of $P^{(3)+}$ due to the destruction of the grating based on the population of the vibrationally relaxed excited electronic state. The term $|A(\tau)|^2$ describes the contribution of the solvation dynamics to the time evolution of the signal.

Let us consider the main physical processes, occurring in a solvating system under a laser excitation (Fig. 1). The pump pulses of frequency ω create a hole in the initial thermal distribution relative to the generalized solvation coordinate in the ground electronic state and, simultaneously, a spike in the excited electronic state. Apparently, such formations have a space modulation $\sim \exp[-i(\boldsymbol{k}_1 - \boldsymbol{k}_2)\cdot\boldsymbol{r}]$. These distributions tend to the equilibrium point of the corresponding potentials over time, and are also broadened during their movements. These changes are measured by the probe pulse delayed by a time τ relative to the pump pulses.

[#1] This assumption might be wrong for slow isomerization and conformer intramolecular transitions as well as for low frequency intramolecular vibrations [56]. However, the contribution of low frequency intramolecular vibrations to the whole attenuation of a nonequilibrium state was found to be 20 times weaker than the fast component with a decay time of 60 fs attenuation [56]. The contribution of these low frequency vibrations to the signal can be explained by non-Condon mechanisms [57]. As to isomer and conformer transitions, for LDS dyes the isomerization time is rather long ($\gtrsim 50$ ps). We shall discuss in detail this issue in the discussion section of the paper. Concerning the two stages of a molecular relaxation in solutions (fast-intramolecular and slower-intermolecular one) see refs. [55,58].

Let us adduce at first the formula for $A(\tau)$ without taking into account the intramolecular degrees of freedom [40]:

$$A(\tau) \sim F^{e}_{S\alpha}(\omega-\omega_{21}) \times\Big(F_{S\alpha}(\omega-\omega_{\alpha},\tau)+F_{S\varphi}(\omega-\omega_{\varphi},\tau) +\mathrm{i}\frac{2}{\sqrt{\pi}}[X_{S\alpha}(\omega-\omega_{\alpha},\tau)+X_{S\varphi}(\omega-\omega_{\varphi},\tau)]\Big), \tag{16}$$

where "e" means the equilibrium value. The formula completely corresponds to the physical processes taking place in solvation of the system considered before. The value of $A(\tau)$ depends on changes related to nonequilibrium solvation processes in both the $F_{\alpha,\varphi}$ absorption (α) and the emission (φ) spectra [40],

$$F_{S\alpha,\varphi}(\omega-\omega_{\alpha,\varphi},\tau) = \frac{1}{\sqrt{2\pi\sigma(\tau)}}\exp\{-[\omega-\omega_{\alpha,\varphi}(\tau)]^2/2\sigma(\tau)\}, \tag{17}$$

at the active pulse frequency ω, as well as on the corresponding changes in both the spectra of the refraction index $X_{S\alpha,\varphi}(\omega-\omega_{\alpha,\varphi},\tau)$. $X_{S\alpha,\varphi}$ are related to $F_{S\alpha,\varphi}$ by the Kramers–Kronig formula, and have the following form [40]:

$$X_{S\alpha,\varphi}(\omega-\omega_{\alpha,\varphi},\tau) = F_{S\alpha,\varphi}(\omega-\omega_{\alpha,\varphi},\tau)\ \mathrm{Erfi}\left(\frac{\omega-\omega_{\alpha,\varphi}(\tau)}{[2\sigma(\tau)]^{1/2}}\right).$$

where

$$\mathrm{Erfi}(x) = \int_0^x \exp(y^2)\,\mathrm{d}y .$$

As can be seen from Eq. (17), the changes in both spectra $F_{S\alpha,\varphi}$ at each instant in time τ are Gaussian functions with time dependent width proportional to $[2\sigma(t)]^{1/2}$

$$\sigma(\tau) = \sigma_{2S}[1-S^2(\tau)] . \tag{18}$$

Thus, as follows from Eq. (18) the width of the light-induced changes in both spectra are small for small delay times τ ($S(\tau)\approx 1$). The hole and the spike distribution broaden in time relative to the solvation coordinate (Fig. 1a).

The detuning $\omega-\omega_{\alpha,\varphi}(\tau)$ of $F_{S\alpha,\varphi}$ are functions of the delay time τ [40]:

$$\omega_{\alpha}(\tau) = \omega_{21} + (\omega-\omega_{21})S(\tau) ,$$
$$\omega_{\varphi}(\tau) = (\omega_{21}-\omega_{St}) + (\omega-\omega_{21}+\omega_{St})S(\tau) . \tag{19}$$

The detuning $\omega-\omega_{\alpha}(\tau)$ is connected with the motion of the hole in time, and the detuning $\omega-\omega_{\varphi}(\tau)$ depends on the motion of the spike (Fig. 1a). The values $X_{S\alpha,\varphi}(\omega-\omega_{\alpha,\varphi},\tau)$, which are related to $F_{S\alpha,\varphi}(\omega-\omega_{\alpha,\varphi},\tau)$ by the Kramers–Kronig formula, display the corresponding changes in the index of refraction.

Now, let us take into account the intramolecular vibrations. In this case the adiabatic potentials will be represented by hypersurfaces (Fig. 1b). The corresponding absorption and emission spectra will be represented by the convolutions

$$F^{e}_{\alpha}(\omega-\omega_{21}) = \int \mathrm{d}\omega'\, F_{M}(\omega')F_{S\alpha}(\omega-\omega_{21}-\omega') , \tag{20a}$$

$$F^{e}_{\varphi}(\omega_{21}-\omega_{St}-\omega) = \int \mathrm{d}\omega'\, F_{M}(\omega')F_{S\varphi}(\omega_{21}-\omega_{St}-\omega-\omega') . \tag{20b}$$

The shape of the "intramolecular" spectrum $F_{M}(\omega')$ is determined schematically by the 1-D potentials $U_1(Q_M, 0)$ and $U_2^{FC}(Q_M)$ (Fig. 1b) that are obtained by the intersection of the hypersurfaces $U_2(Q_M, Q_S)$ and $U_1(Q_M, Q_S)$ by a vertical plane passing through the "molecular" coordinate Q_M:

$$F_{M}(\omega') = (2\pi)^{-1}\int_{-\infty}^{\infty}\mathrm{d}t\,\exp[g_{M}(t)-\mathrm{i}\omega' t] . \tag{21}$$

The "intermolecular" spectrum $F_{S\alpha}(\omega-\omega_{21}-\omega')$ is determined by "1-D" potentials that are obtained by the intersection of the hypersurfaces by a vertical plane passing through the solvation coordinate Q_S. The situation is similar for the emission spectrum. Typical "intramolecular" and whole spectra are shown in Fig. 2.

We now calculate $A(\tau)$ in the general "2-D" case where both the intramolecular and intermolecular contributions are taken into account. The calculation is the

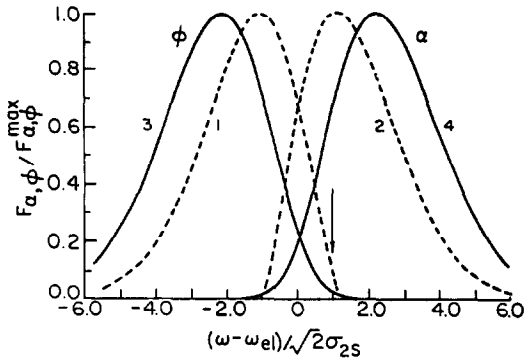

Fig. 2. The shape of the "intramolecular" spectra $F_M(\omega')$. 1 and 2 are the equilibrium luminescence and absorption spectra of a molecule, respectively, when the solvent contribution from the solvent is absent; 3 and 4 are the equilibrium spectra of a molecule in solution. The arrow shows the relative position of excitation frequency ω for the four-photon signal calculation (Fig. 3).

generalization of the results [40] for the case of an arbitrary spectrum $F_M(\omega')$, corresponding to the reorganization of the ultrafast intramolecular degrees of freedom during the electron transition.

In the general case the value of $A(\tau)$ is represented by the 2-D integral:

$$A(\tau) = \int\int d\omega'\, d\omega''\, F_M(\omega'') F^e_{S\alpha}(\omega-\omega_{21}-\omega'') \times\Big(F_{S\alpha}(\omega-\omega_\alpha,\tau)+F_{S\varphi}(\omega-\omega_\varphi,\tau) + i\frac{2}{\sqrt{\pi}}[X_{S\alpha}(\omega-\omega_\alpha,\tau)+X_{S\varphi}(\omega-\omega_\varphi,\tau)]\Big), \quad (22)$$

which does not reduce to the product of the one-dimensional integrals (according to Eq. (20)). The reason is that the frequencies $\omega_{\alpha,\varphi}$ in Eq. (22) are functions of both ω' and ω'':

$$\omega_\alpha(\tau) = (\omega_{21}+\omega') + (\omega-\omega_{21}-\omega'')S(\tau),$$
$$\omega_\varphi(\tau) = (\omega_{21}-\omega'-\omega_{St}) + (\omega-\omega_{21}-\omega''+\omega_{St})S(\tau). \quad (23)$$

The physical reason for such a dependence is given by the following arguments. Let us return to Fig. 1a. The situation that is shown in this figure is characteristic also for the "2-D" case, however, it is true only for the intersections of hypersurfaces by the vertical plane passing through the coordinate Q_S (Fig. 1b). Therefore, any distribution shown in Fig. 1a will be accompanied by the equilibrium distribution with respect to the "intramolecular" coordinate Q_M.

Let us consider for the definition only the processes corresponding to the second and the fourth addends in Eq. (22). The pump pulses act along the transition α between the "plane" potentials $U_1(Q_M, 0)$ and $U_2^{FC}(Q_M)$ (Fig. 1b), bearing the spike of the distribution on the bottom of the Franck–Condon potential $U_2^{FC}(Q_M)$ (point A) due to the instantaneous intramolecular relaxation. If the delay time τ of the probe pulse is small with comparison to the relaxation time with respect to the coordinate Q_S, the probe pulse will act also between the potentials $U_2^{FC}(Q_M)$ and $U_1(Q_M, 0)$ and, correspondingly, the spectra $F_M(\omega')$ and $F_M(\omega'')$ in Eq. (22) will be strongly correlated. For large delays τ, the spike will relax to the equilibrium state (point B). Therefore, the probe pulse will probe a peculiarity in the range of the pair of potentials: $U_2(U_M, d_S)$ and $U_1^{FC}(Q_M)$ (the transition φ). The corresponding spectra $F_M(\omega')$ and $F_M(\omega'')$ will not correlate. In this case the double-integration reduces to the product of 1-D integrals, i.e. to the product of the corresponding equilibrium spectra.

Figs. 3 illustrate the time behavior of the signal $J_S(\tau)$ that was calculated by formulae (15), (17)–(23). The shape of the "intramolecular" spectrum $F_M(\omega')$ is modeled by a "smoothed" dependence of one optically active intramolecular vibration of frequency ω_0 [59,60]: $F_M(\omega') \sim \bar{S}^x/\Gamma(x+1)$ where $\Gamma(x+1)$ is the gamma-function, $x=(\omega'-\omega_{el})/\omega_0$, $\omega_{el}=(E_2^0+\langle V_2^{el}\rangle - E_1^{el}-\langle V_1^{el}\rangle)/\hbar$ is the frequency of the purely electronic transition of a molecule in solution. We used the following values for the parameters: $\omega_{St}(2\sigma_{2S})^{-1/2}=2$, $\bar{S}=1.5$, $\omega_0(2\sigma_{2S})^{-1/2}=1.14$. The shape of the "intramolecular" spectrum $F_M(\omega')$ for these parameters is shown in Fig. 2 in the form of the equilibrium spectra $F^e_\alpha(\omega-\omega_{el})$ and $F^e_\varphi(\omega_{el}-\omega)$ when the contribution from the solvent is absent. $F^e_\alpha(\omega-\omega_{el})$ and $F^e_\alpha(\omega_{el}-\omega)$ are determined by formulae (20) for the substitutions $\omega_{21}\to\omega_{el}$, $\omega_{St}=0$, $F_{S\alpha}\to\delta(\omega-\omega_{el}-\omega')$ and $F_{S\varphi}\to\delta(\omega_{el}-\omega-\omega')$, $\delta(x)$ is the δ-function of Dirac. The equilibrium spectra of the molecule in solution $F^e_\alpha(\omega-\omega_{21})$ and $F^e_\varphi(\omega_{21}-\omega_{St}-\omega)$ are also shown in Fig. 2.

It follows from Eqs. (15) and (22) that the signal $J_S(\tau)$ depends on the excitation frequency ω. We chose $\omega=\omega_{el}+\omega_{St}/2$, which approximately corresponds to

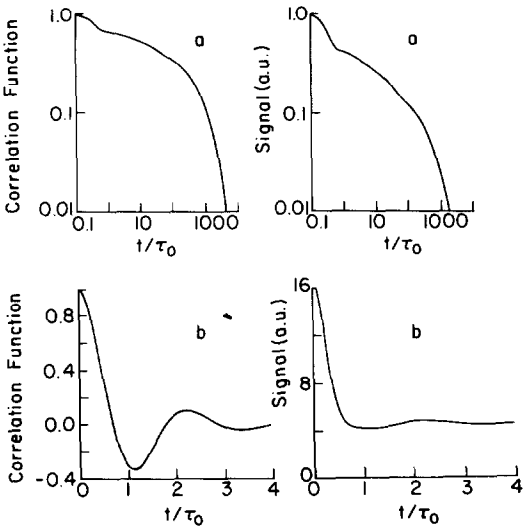

Fig. 3. Model calculations of the RTGS signal: (a) the solvation correlation function consists of a Gaussian followed by three exponential decay (Eq. (17a)), note the curves are on a logarithmic scale. (b) the correlation function corresponds to a Brownian oscillator model for the liquid behavior (Eq. (17b)); $\tau_0 = 200$ fs, $T_1/\tau_0 = \infty$. (a) $a_3\tau_0^2 = 7.7016$, $a_1\tau_0 = 0.33$, $a_5\tau_0 = 0.04$, $a_2 = 0.3$, $a_4 = a_6 = a_8 = 0.2$, $a_7\tau_0 = 0.00074$; (b) $\Gamma\tau_0 = 1$, $\Omega\tau_0 = 2.83$.

the experimental situation (see below). The excitation frequency ω is also shown in Fig. 2.

We used two forms for the correlation function $S(t)$,

$$S(t) = a_2 \exp(-a_3 t^2) + (1 - a_2 - a_4 - a_6 - a_8) \exp(-a_1 t) + a_4 \exp(-a_5 t) + a_6 \exp(-a_7 t) + a_8 \exp(-a_9 t) \quad (24a)$$

and

$$S(t) = \exp(-\Gamma|t|) \times [\cos(\Omega t) + (\Gamma/\Omega) \sin(\Omega|t|)] , \quad (24b)$$

corresponding to a Brownian oscillator [13,45,46,61–63].

The first addend in expression (24a) for the first correlation function corresponds to a fast Gaussian component, observed in ref. [12]. The second one corresponds to the relatively fast exponential component with an attenuation time of 200–400 fs observed in ref. [12] and in our experiment (see below). The third component corresponds to a slower attenuation with a decay time of the longitudinal relaxation τ_L. It is worth noting that such a division by different contributions to the correlation function is purely formal, and is used here to impart the realistic form of the correlation function. As a matter of fact, both the short- and the long-time components of the correlation function are manifestations of one physical process. We shall discuss this issue in more detail below. We also showed in Figs. 3 the time dependence of the correlation functions $S(\tau)$, used for the calculation of corresponding signals $J_S(\tau)$.

One can see that the dependencies $S(\tau)$ and $J_S(\tau)$ are very similar (but not identical), and the signal $J_S(\tau)$ reflects the fine details of $S(\tau)$. Thus, the RTPGS can be used for the ultrafast study of the solvation dynamics.

The dependence of the signal $J_S(\tau)$ on the excitation frequency ω is investigated in ref. [64].

Comparison of RTPGS with pump–probe spectroscopy. In transmission "pump–probe" experiments [56] the dependence of the change in the sample transmission ΔT on the delay time τ between pump and probe pulses is measured. This dependence is given by [48,57]

$$\Delta T(\tau) \sim -\mathrm{Re} \int_{-\infty}^{\infty} \mathrm{d}t\, E^{-}_{\mathrm{probe}}(t-\tau) \times \frac{\mathrm{d}}{\mathrm{d}t} [P^{(3)+}(t) \exp(-\mathrm{i}\omega t)] . \quad (25)$$

For the above-mentioned assumptions we obtain

$$\Delta T(\tau) \sim \omega \exp(-\tau/T_1)\ \mathrm{Re}\, A(\tau) , \quad (26)$$

where $A(\tau)$ is determined by Eq. (22). The comparison of Eq. (26) for $\Delta T(\tau)$ with Eq. (15) for $J_S(\tau)$ shows that the signal in pump–probe spectroscopy is determined by the same physical processes as for RTPGS. However, in contrast to the latter, $\Delta T(\tau)$ does not depend on the refraction index $X_{\alpha,\varphi}$ spectra.

Comparison of RTPGS with TRL spectroscopy. The relaxation processes of an excited molecule are observed by both techniques, the TRL and the TRPGS. Since the signal in TRPGS is determined by the population grating (which includes the contribution of both the space modulation of the electronic level populations and the space modulation of the vibrationally nonequilibrium populations), it must be closely related to the

TRL signal that is also determined by the electronic and the vibrational populations.

The equation describing the dependence of the TRL $G^f(\nu, \omega, \tau)$ on the radiated frequency ν, the excitation frequency ω, and the time τ after excitation is given by [51]

$$G^f(\nu, \omega, \tau) = \int\int d\omega' \, d\omega'' \, F_M(\omega')F_M(\omega'') \times F^e_{S\alpha}(\omega - \omega_{21} - \omega'')F_{S\varphi}(\nu - \omega_\varphi, \tau) \, . \quad (27)$$

Eq. (26) is correct when the intramolecular relaxation is much faster than the solute-solvent one [51]. One can easily see that Eq. (26) coincides with the second term in the right-hand side of Eq. (22) for $A(\tau)$ when $\nu = \omega$. Thus the transient luminescence spectrum provides a contribution to the observed signal of RTPGS. We would like to emphasize, that the molecular model we presented is the same for RTPGS and TRL.

There are three main differences between the RTPGS and the TRL spectroscopy. First in luminescence, the whole spectrum is measured while in RTPGS only the excitation frequency is monitored. Second, the RTPGS monitors both the excited state and the ground electronic state relaxation. Third, in the RTPGS experiment the refraction index spectra of the ground and excited states also contribute to the signal.

3. Experimental details

The laser source consists of a cw mode-locked Nd:YAG laser (Coherent Antares) operating at 76 MHz. A small portion of the 1.06 μm radiation (~20 mW) is used to seed a cw Nd:YAG regenerative amplifier operating at 500 Hz. The regenerative amplifier output pulses of 1.1 mJ energy at 1.06 μm are doubled with a beta barium borate (BBO) crystal and reach and energy per pulse of 0.4 mJ at 532 nm. The doubled frequency output of the amplifier (70 ps full width half maximum) was used to amplify the ultrashort laser pulse 140 fs fwhm, 1 nJ generated by a synchronously pumped dye laser. The synchronously pumped dye laser (Satori, Coherent) utilizes a saturable absorber in combination with group velocity dispersion compensation prisms to achieve a stable pulse width of the order of 140 fs. The dye amplifier consists of three flowing dye cells pumped by the regenerative amplifier second-harmonic pulse. With Kiton red dye the dye laser operates at 635 nm central wave length and the amplification is achieved by DCM dye to ~15 μJ with a pulse width comparable with the non-amplified pulse.

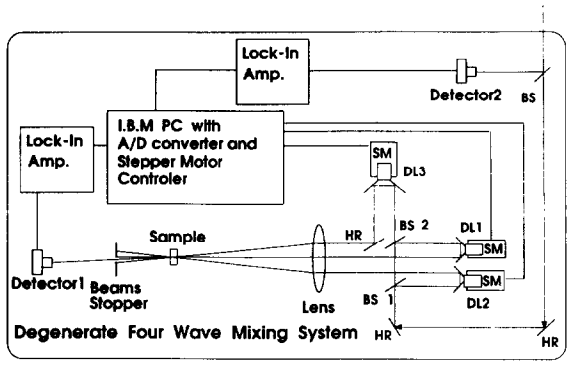

Fig. 4. The schematics of the optical setup for time-resolved degenerate four-wave mixing experiments. BS: beam splitter. DL: delay line, SM: step motor. HR: high reflector.

The four-wave mixing optical setup is shown in Fig. 4. The amplified (15 μJ) 140 fs laser pulse was split into three beams. Optical delay lines were used to overlap in time the pump beams and to control the time delay of the probe beam. The three beams (parallel polarization) were focused onto the sample by a single lens of 50 cm focal length. In DFWM experiments the signal beam exit the sample at a unique direction $\boldsymbol{k}_S = (\boldsymbol{k}_1 - \boldsymbol{k}_2) + \boldsymbol{k}_3$ and therefore it is easily separated from the three generation beams.

LDS 750 (styryl 7) was purchased from Exciton and was used without further purification. The solvents used were either analytical or of a spectroscopical grade. Samples were circulated in a flowing cell of 1 mm pathlength.

4. Experimental results

The time-resolved four-wave mixing signal was measured by the experimental setup shown in Fig. 4. The time dependent four-wave mixing signals of LDS 750 in methanol, 1,2-ethanediol, 1,3-propanediol and 1,4-butanediol are shown in Fig. 5. The absorption and emission spectra of LDS 750 in 1,3-propanediol are shown in Fig. 6. The signals were collected with a relatively low time resolution by scanning the probe beam delay stage at 0.5 ps steps. As seen from Fig. 5 the signal decay curves for LDS 750 in these solvents

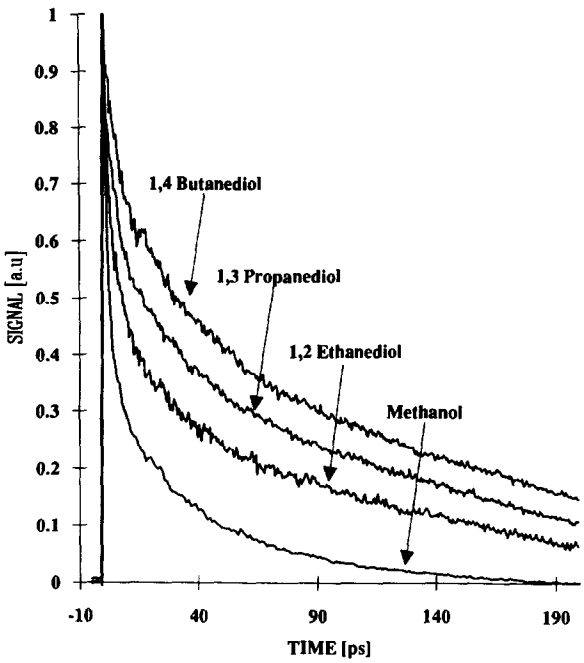

Fig. 5. Degenerate four-wave mixing signal of LDS 750 in various solvents as a function of time delay between the pump pulses and the probe pulse: from top to bottom, 1,4-butanediol, 1,3-propanediol, 1,2-ethanediol and methanol.

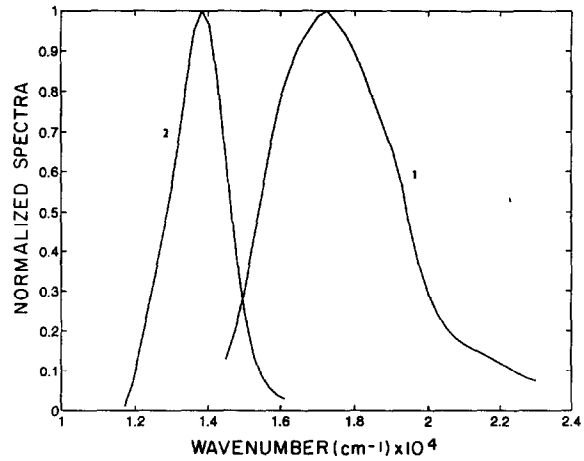

Fig. 6. The absorption (1) and luminescence (2) spectra of LDS 750 in 1,3-propanediol.

are nonexponential and consist of several time domains. The long life time component in methanol exhibit an exponential decay law with corresponding life times of 120 ps. This life time we attribute to the electronic population grating attenuation. The fluorescence lifetimes of LDS 750 in methanol 1,2-ethanediol, 1,3-propanediol and 1,4-butanediol are 240 ps [11], 600, 900 and 1100 ps respectively. The factor of two between the electronically excited state lifetime measured by luminescence technique and the longest decay of the DFWM signal arises from the following argument. The signal in DFWM experiments is proportional to $|P^{(3)+}|^2$ ($P^{(3)}$ is the cubic polarization). If population gratings are formed in such experiments then $P^{(3)+}$ decay as $\exp(-\tau/T_1)$ where T_1 is the excited state lifetime. However, the DFWM signal decays as $\exp(-2\tau/T_1)$. Thus the decay rate constant of a population grating in a DFWM experiment is twice as large as the actual decay rate constant of the excited state population.

The shorter time components of the DFWM signal of LDS 750 in methanol, and the diols are seen on a shorter time scale with an expanded time resolution (100 fs time steps) in Fig. 7. Each of the decay curves shown in Fig. 7 consists of three time components. We attribute all these time components to the solvation dynamics of LDS 750.

The longest component can be approximately fitted to an exponential decay with decay times of 5, 10, 30

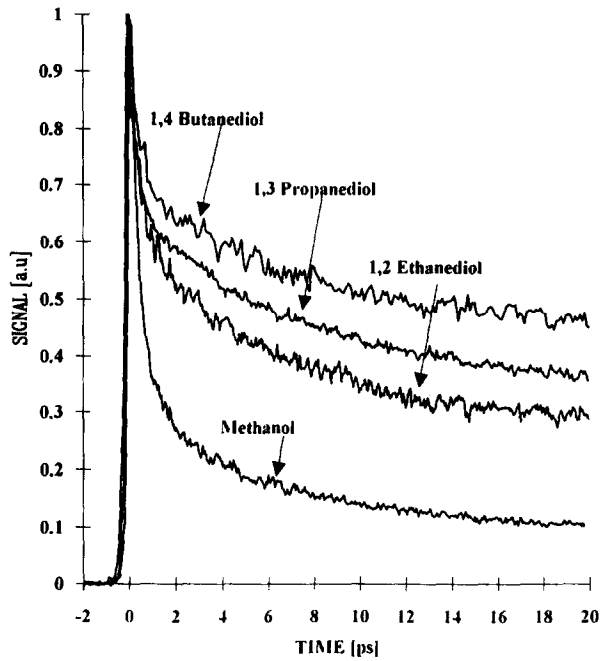

Fig. 7. DFWM signal of LDS 750 in four solvents measured by delay line steps of 100 fs.

and 70 ps for methanol, 1,2-ethanediol, 1,3-propanediol and 1,4-butanediol, respectively. These relaxation times correspond to the longitudinal dielectric relaxation time τ_L of the particular liquid. The dielectric relaxation properties of monoalcohols were studied quite extensively [65,66]. While the dielectric relaxation time τ_D is obtained for measurements that senses the orientational motion of the liquid molecules at constant field, the longitudinal relaxation time τ_L provides the liquid relaxation time at constant charge. The two relaxation times are related by a simple formula $\tau_L = (\varepsilon_\infty/\varepsilon_S)\tau_D$ where ε_S and ε_∞ are the low and high frequency dielectric constant respectively. The constant charge, longitudinal relaxation time is more appropriate to compare with the solvation dynamics of excited solute molecules [1,3,6].

The dielectric relaxation properties of neat normal primary alcohols present a complex behavior. This complexity is attributed to the hydrogen bonding between adjacent molecules. The relatively long relaxation time is attributed to the breaking of hydrogen bonds in molecular aggregates followed by ROH rotation. In addition to the long relaxation component, shorter relaxation times are observed in alcohols. Since the dielectric relaxation measurements are frequency limited by the instrument response, the high frequency dielectric response obtained in these measurements is inaccurate and often not available. Garg and Smyth [65] analyzed their data for propanol to dodecanol in terms of three different relaxation times for each alcohol. They explained the intermediate relaxation time as arising from rotation of a free monomeric molecule. The shortest relaxation time is that for the relaxation of the hydroxyl group by rotation around its C–O bond. It was estimated to be ~2 ps and was found to be insensitive to the particular liquid.

The dielectric spectra of diols are unsymmetrical. The Cole–Cole plots are skewed ones over most of the dispersion range [67]. Various relaxation model functions have been assumed in earlier work on diols. In early investigations of dielectric spectra of liquids few frequencies and rather limited frequency ranges have been used to characterize the spectra and therefore the differentiation between model functions was difficult. In more recent studies of linear 1,2-diols by El-Samahy and Gestblom [68] (using dielectric time domain spectroscopy) and Jordan et al. [69] (using spot frequency domain measurements between 10 MHz and 70 GHz) it was found significantly better fit to their data assuming two Debye relaxation times rather than model functions like Cole–Davidson distribution or Cole–Cole distribution. The two dielectric relaxation times for 1,2-ethanediol are 140 and 20 ps [68]. The long relaxation time is approximately the same as for ethanol. In monoalcohols like methanol, τ_{D2} the shorter decay time is generally interpreted in terms of a monomer reorientation while τ_{D1} represents a cooperative motion connected with the breakup of hydrogen bonds inside a polymeric alcohol unit. The similarity in the dielectric spectra of mono and dialcohols indicates analogous behavior. However, in diols τ_{D2} increases more pronouncely with the molar mass than for monoalcohols. In contrast the longer relaxation time τ_{D1} is less sensitive to the chain length than the corresponding monoalcohols.

The short time components of the DFWM signals of LDS 750 in methanol and the diols solutions are shown in Fig. 8, using 20 fs time steps of the probe beam delay stage. The DFWM signal for both solvents consists of an ultrashort spike followed by a ~400 fs (methanol) and a <400 fs decay for the diols. The initial Gaussian shape spike is due to a contribution of two superim-

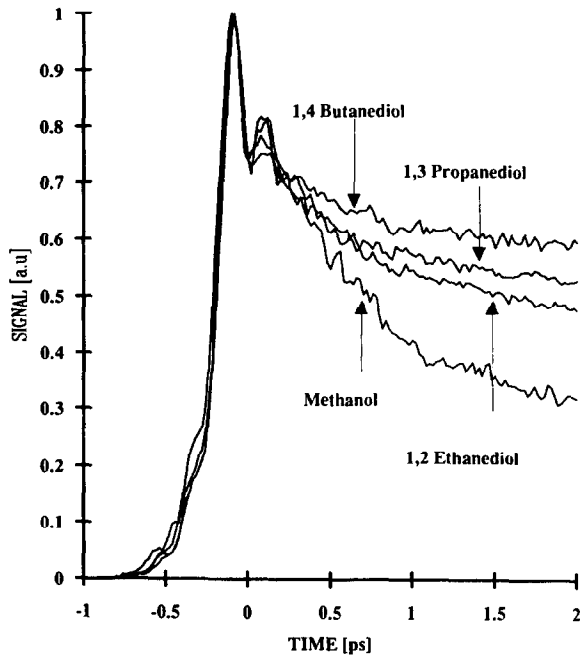

Fig. 8. High time resolution DFWM signal of LDS 750 in four solvents measured with time steps of 20 fs.

posed components. A coherent contribution arises due to repumping of energy from the pumping beams to the probe beam and is often found in DFWM experiments. The coherent spike fwhm is determined by the laser pulse correlation function and hence by the laser pulse width. The coherent spike prevents us for the time being to resolve accurately the first ~ 150 fs of the solvation dynamics.

The ultrafast solvation dynamics of LDS 750 in acetonitrile was studied by Rosenthal et al. [12] using time resolved luminescence technique with ~ 125 fs fwhm instrument response function. The solvation response consisted of two distinctive parts. A fast initial decay accounted for ~ 80% of the amplitude was fit by a Gaussian. The slower tail decayed exponentially with a decay time of 200 fs. In a subsequent study, Cho et al. [13] measured the time-dependent nonresonant optical Kerr effect in neat acetonitrile liquid. Both experiments have shown the biphasic character of the solvent response. A vibrational model was used to describe quantitatively the solvation and the neat liquid dynamics [13]. A number of Brownian oscillators with frequency distribution of the vibrational modes produce a very good fit of both experimental data.

The shortest time component has a Gaussian shape (see Fig. 8) but cannot be time resolved since the coherent spike is superimposed on it. Also the pulse duration in our experiment is longer than the predicted Gaussian component of the solvation. We now wish to compare the solvation dynamics on the short time scale < 2 ps of LDS 750 in methanol, and the diols. On this short time scale the solvation dynamics in all solvents is quite similar. The relative height of the coherent spike superimposed on the Gaussian compound versus the subsequent total signal is the same in all three liquids (see Fig. 8). The decay time of the exponential component is ~ 400 fs in MeOH and longer in diols. This decay time is about twice as longer than in acetonitrile [12,13]. It is interesting to note that while the longer solvation components in these liquids are strongly dependent on the particular liquid, the ultrafast solvation dynamics is almost identical (within the S/N ratio of the experimental data).

However relative amplitude of the ~ 400 fs component is ~ 0.4 for methanol and drastically smaller in the diols (0.2, 0.15 and 0.1 in 1,2-ethanediol, 1,3-propanediol and 1,4-butanediol, respectively).

The solvation dynamics of probe molecules in associated liquids is quite complex and spans several time decades. In order to follow accurately the solvation

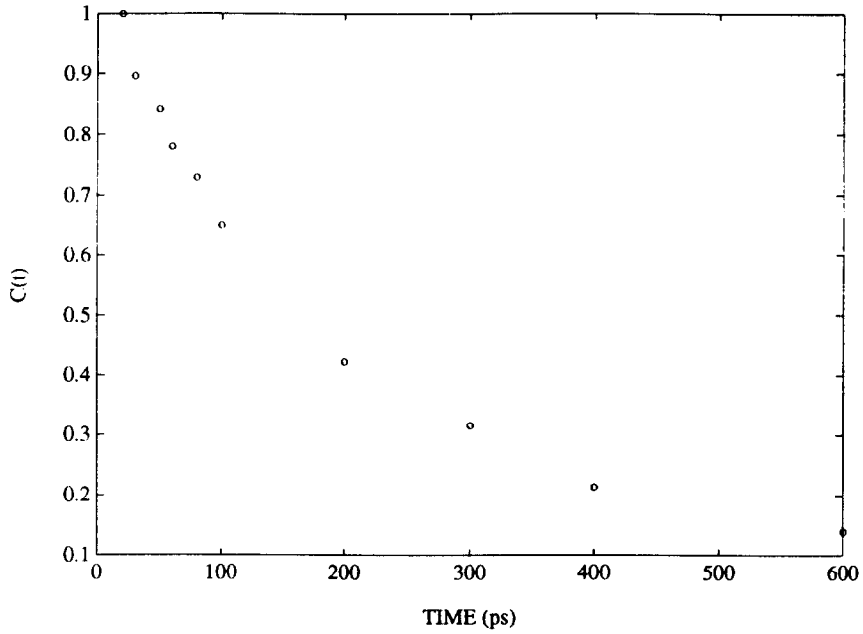

Fig. 9. The solvation correlation function of LDS 750 in 1,4-butanediol measured by time-resolved emission technique.

dynamics on the subnanosecond time scale we measured the time resolved fluorescence of LDS 750 in methanol and in the diols. Time correlated single photon counting technique with 50 ps instrument response was used to follow the solvation correlation function $S(t)$ (see Eqs. (23) and (27)) at times longer than $\gtrsim 30$ ps. The combination of both methods RTPGS limited by our delay lines to time shorter $\leqslant 200$ ps and the TCSPC limited by the instrument response $\geqslant 30$ ps, increases the time range, the time resolution and the signal to noise ratio of the experimental data. Fig. 9 displays the solvation correlation function obtained from the time resolved spectra of LDS 750 in 1,4-butanediol constructed from TCSPC data. The approximate solvation function from ~ 100 fs to ~ 1 ns on a logarithmic scale is shown in Fig. 10.

Using the similarity of the RTPGS signal and the correlation function (Fig. 3), the signals shown in Fig. 10 were constructed as follows. The four-wave mixing signals with high, medium and low time resolution of a particular solvent (see Figs. 5, 7 and 8) were added together to construct the signals shown up to ~ 100 ps. The time resolved emission of LDS 750 at 650 nm was added to complete the signal up to 1000 ps (we used the single wavelength method for the determination of the correlation function [74]). The total signal (in order to exclude the attenuation) was then multiplied by $\exp(t/\tau_1)$ where T_1 is the excited state life time and finally the relaxed emission was subtracted from the signal. The processes signals displayed in Fig. 10 provide the high time resolution necessary to define the initial solvation components as well as the slowest components in one curve.

The solvation dynamics shown in Fig. 10 is complex and it occurs on four time decades < 100 fs to several hundred picoseconds. For LDS 750 in 1,4-butanediol using a Gaussian and four exponential fit the characteristic times involved in the solvation dynamics are: a Gaussian component with a relative amplitude 0.3 and time of < 100 fs, a small component with an amplitude of 0.1 and a decay time of ~ 600 fs followed by 5 ps, 70 ps and ~ 250 ps components with amplitudes of ~ 0.15, 0.15 and 0.15 respectively.

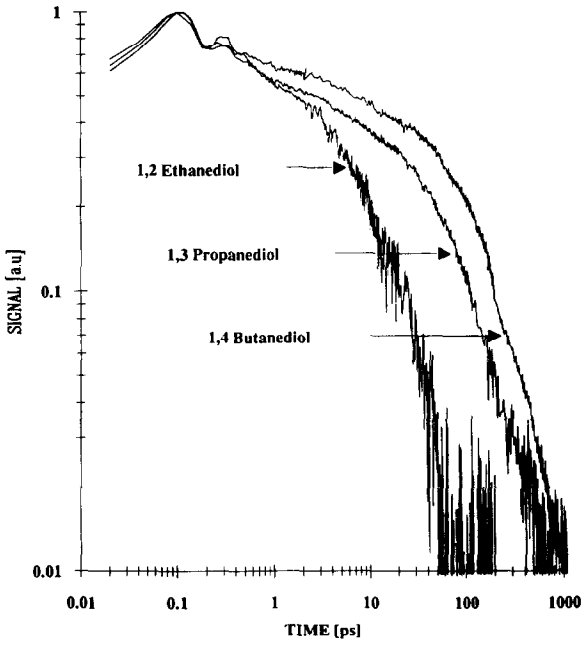

Fig. 10. Solvation dynamics of LDS 750 in three diols presented on a logarithmic scale. Note: The solvation dynamics is displayed on four decades of time.

5. Discussion

In the present study we continue our efforts to understand the solvation dynamics of large probe molecules. To probe the relative merits of viscosity and solvent relaxation time in solvation dynamics of LDS 750, we have utilized the fact that in diols the two parameters do not scale linearly with the corresponding values of monoalcohols. The diols have larger dipole moment and larger viscosities than monools (1,2-ethanediol, μ, 2D, η, 19 cP; ethanol, μ, 1.7D, η, 1.2 cP). In contrast, the longer dielectric relaxation times measured by electrical relaxation methods are about the same (140 ps for 1,2-ethanediol and 120 ps for ethanol [68–71]. In the study of solvation dynamics and intramolecular electron transfer processes, monoalkanols scale almost linearly with viscosity and the relative utility of the two parameters in evaluating solvation dynamics was not easily clarified.

Time resolved four-wave mixing method provided the solvation dynamics of LDS 750 on the short and medium time scales ~ 100 fs–200 ps. The four-wave mixing data between ~ 50 and 200 ps match quite

nicely to the solvation dynamics measured by time resolved fluorescence measurements (see Fig. 10). The solvation dynamics complexity is clearly seen in Fig. 10. For simplicity, we analyzed the experimental curves by a Gaussian component followed by four exponents where the longest one we attribute to the excited state life time.

In all solvents the superimposed coherent spike and the Gaussian component have the same relative amplitude ~ 0.3.

The relative amplitude of the first exponential component is strongly dependent on the solvent. For methanol, the relative amplitude is ~ 0.4 while for 1,4-butanediol ~ 0.1. The decay time constants of the shortest exponent are 400–600 fs. It is difficult to determine the exact rate since the relative amplitude is small and the exponential analysis serves only as a guideline to quantify the complex relaxation.

As mentioned previously, the dielectric relaxation measurements indicated that in monoalcohols ultrafast dielectric relaxations of the order of ~ 2 ps exists while for 1,2-ethanediol the shortest component found is ~ 20 ps. Our solvation dynamics experiments show that the time scale of the fastest solvation components for monools and diols are much shorter. In all solvents it consists of a Gaussian component of $\leqslant 100$ fs followed by a ~ 400 fs exponential decay. Molecular dynamics simulations of solvation dynamics in methanol [29] have shown that the solvation dynamics is biphasic. A Gaussian contribution with < 100 fs is identified as arising from the inertial rotational motion of the solvent molecules. The second component is longer and approximately decays exponentially with 400 fs decay time. Classical molecular dynamics simulation of methanol [31] performed to much longer times (10 ps) than the solvation simulations work [29] 1 ps shows the long solvation component of 5 ps (found in our experiment) as well as the short components. The ultrafast solvation components can be deduced from far infrared absorption measurements [33,34]. The Fourier transform of the far-infrared absorption line shape of neat acetonitrile and acetonitrile in other liquids shows both the Gaussian and the exponential components of the solvent orientational correlation function. The second exponential rate constant is strongly dependent on the solvent. For methanol it corresponds to τ_{D1}. In the diols the second exponent is followed by a longer decay which corresponds to the longest dielectric relaxation time τ_D, measured by electrical measurements via the longitudinal relaxation time $\tau_L = (\varepsilon_\infty/\varepsilon_S)\tau_D$.

Bearing in mind the possibility that two isomers of LDS 750 [72] exists, let us discuss this in the framework of our theory. The generalization of the theory for the case of a few isomers is direct. One must calculate the values $A_i(\tau)$ for each isomer, and the TRPGS signal $J_S(\tau)$ (Eq. (4)) is given by

$$J_S(\tau) \sim \left| \sum_i \exp(-\tau/T_{1i}) A_i(\tau) \right|^2 , \qquad (28)$$

where T_{1i} is the lifetime of the excited state for the ith isomer. One can also take into account the transitions between isomers, but they are relatively slow processes [72]. We shall conduct such a generalization in the future.

In this work we developed theoretically and experimentally the principles of a new method for the observation of ultrafast solvation dynamics: the resonance transient population grating spectroscopy. Theoretical results reproduce the main properties of the experimental curves.

The theory presented in the paper connects a four-photon signal with the correlation function $S(t)$ that describes the fluctuations of the value $u_S(t)$ and the transient Stokes shift of the luminescence spectrum ($\omega_\varphi(t)$). The analytical form of $S(t)$ can be arbitrary in principal. Its calculation is an independent problem.

There are number of papers devoted to the calculation of $S(t)$. The model of the strongly overdamped Brownian oscillator [63,64] describes only the long-time (exponential) behavior of $S(t)$. The use of a frequency distribution of the solvation modes in the form of Brownian oscillators [13] describes both the fast and the slow components of $S(t)$. However, such a description is rather characteristic for polar crystals than for polar solvents, where the change of the polarization originates from the rotation of the molecules. The approach based on Kubo's stochastic theory [19] that describes both the short and the long components, seems to us rather attractive. However, an approach on the basis of the generalized Langevin equation [61,73] is more consistent. On the basis of this equation we proposed before the non-Markovian model of an optically active oscillator for electron transitions in mole-

cules [61]. We shall use such an approach to describe the solvation correlation function $S(t)$ elsewhere.

Acknowledgement

This work was supported by grants from the Israeli Ministry of Science and Technology, The United States–Israel Binational Science Foundation (BSF) and the James Franck Binational German–Israel Programme in Laser Matter Interaction.

References

[1] E.M. Kosower and D. Huppert, Ann. Rev. Phys. Chem. 37 (1986) 127.
[2] P.F. Barbara and W. Jarzeba, Advan. Photochem. 15 (1990) 1.
[3] M. Maroncelli, J. MacInnis and G.R. Fleming, Science 243 (1989) 1674.
[4] G.R. Fleming and P.G. Wolynes, Phys. Today 43 (1990) 36.
[5] B. Bagchi and A. Chandra, Advan. Chem. Phys. 80 (1991) 1.
[6] D. Huppert, H. Kanety and E.M. Kosower, Discussion Faraday Soc. 74 (1982) 161.
[7] F. Heisel and J.A. Miehe, Chem. Phys. 98 (1985) 233.
[8] J.D. Simon and S.-S. Su, J. Chem. Phys. 87 (1987) 7016.
[9] M.A. Kahlow, W. Jarzeba, T.P. Dubruil and P.F. Barbara, Rev. Sci. Instr. 59 (1988) 1098.
[10] M. Maroncelli and G.R. Fleming, J. Chem. Phys. 89 (1988) 875.
[11] E.W. Castner Jr., M. Maroncelli and G.R. Fleming, J. Chem. Phys. 86 (1987) 1090.
[12] S.J. Rosenthal, X. Xie, M. Du and G.R. Fleming, J. Chem. Phys. 95 (1991) 4715.
[13] M. Cho, S.J. Rosenthal, N.F. Scherer, L.D. Ziegler and G.R. Fleming, J. Chem. Phys. 96 (1992) 5033.
[14] D. Huppert, V. Ittah, A. Masad and E.M. Kosower, Chem. Phys. Letters 150 (1988) 35.
[15] D.A. Wiersma, E.T.J. Nibbering and K. Duppen, in: Ultrafast phenomena VIII, eds. J.-L. Martin, A. Migus, G.A. Mourou and A.H. Zewail (Springer, Berlin, 1993) p. 611.
[16] L.D. Zusman, Chem. Phys. 49 (1980) 295.
[17] B.I. Yakobson and A.I. Burshtein, Chem. Phys. 49 (1980) 385.
[18] H. Sumi and R.A. Marcus, J. Chem. Phys. 84 (1986) 4894.
[19] I. Rips and J. Jortner, J. Chem. Phys. 87 (1987) 2090.
[20] I. Rips, J. Klafter and J. Jortner, J. Chem. Phys. 89 (1988) 4288.
[21] L. Onsager, Can. J. Chem. 55 (1977) 1819.
[22] M.D. Newton and H.L. Friedman, J. Chem. Phys. 88 (1988) 4460.
[23] G. Van der Zwan and J.T. Hynes, J. Phys. Chem. 89 (1985) 4181, and references therein to earlier works.
[24] P.G. Wolynes, J. Chem. Phys. 86 (1987) 5133.
[25] R.F. Loring and S. Mukamel, J. Chem. Phys. 87 (1987) 1272.
[26] B. Bagchi and A. Chandra, J. Chem. Phys. 97 (1992) 5126.
[27] S. Roy and B. Bagchi, in press.
[28] E. Neria and A. Nitzan, J. Chem. Phys. 96 (1992) 5433.
[29] T. Fonseca and B.M. Ladanyi, J. Phys. Chem. 95 (1991) 2116.
[30] L. Perera and M. Berkowitz, J. Chem. Phys. 96 (1992) 3092.
[31] T. Bultmann, K. Kemeter, Ch. Rusbuldt, Ph.A. Bopp and N.P. Ernstig, in: Reaction Dynamics in Clusters and Condensed Phases, 26th Jerusalem Symposium in Quantum Chemistry and Biochemistry, eds. B. Pullman and J. Jortner (Kluwer, Dordrecht, 1994) p. 383.
[32] A. Papazyan and M. Maroncelli, J. Chem. Phys. 98 (1993) 6431.
[33] P.M. Van Aalst, J. Van der Elsken, D. Frenkel and G.W. Wegdam, Faraday Discussions Chem. Soc. 6 (1972) 94.
[34] W.G. Rothschild, Dynamics of molecular liquids (Wiley–Interscience, New York, 1984).
[35] R. Kubo, in: Fluctuation, relaxation and resonance in magnetic systems, ed. D. ter Haar (Oliver and Boyd, Edinburgh, 1962) p. 23.
[36] Y.R. Shen, The principles of nonlinear optics (Wiley, New York, 1984).
[37] Y. Ishida and T. Yajima, Rev. Phys. Appl. 22 (1987) 1629.
[38] A.M. Weiner, S. DeSilvestri and E.P. Ippen, J. Opt. Soc. Am. B 2 (1985) 654.
[39] B.D. Fainberg, Opt. Spectry. 60 (1986) 74.
[40] B.D. Fainberg, Opt. Spectry. 68 (1990) 305.
[41] S.Y. Goldberg, D. Pines, A. Meltsin, B. Fainberg and D. Huppert, Nonlin. Opt. 5 (1993) 307.
[42] B. Fainberg, Phys. Rev. A 48 (1993) 849.
[43] R.F. Loring, Y.J. Yan and S. Mukamel, J. Chem. Phys. 87 (1987) 5840.
[44] B.D. Fainberg, Opt. Spectry. 58 (1985) 323.
[45] B.D. Fainberg and I.B. Neporent, Opt. Spectry. 61 (1986) 31.
[46] B.D. Fainberg and I.N. Myakisheva, Soviet J. Quantum Electron. 17 (1987) 1595.
[47] S. Mukamel, Phys. Rev. A 28 (1983) 3840; J. Phys. Chem. 89 (1985) 1077.
[48] B.D. Fainberg, Chem. Phys. 148 (1990) 33.
[49] J.-Y. Bigot, M.T. Portella, R.W. Schoenlein, C.J. Bardeen, A. Migus and C.V. Shank, Phys. Rev. Letters 66 (1991) 1138.
[50] T. Joo and A.C. Albrecht, Chem. Phys. 173 (1993) 17.
[51] Yu.T. Mazurenko, Opt. Spectry. 48 (1980) 388.
[52] G. Cramer, Mathematical methods of statistics (Princeton Univ. Press, Princeton, 1946).
[53] B.D. Fainberg and B.S. Neporent, Opt. Spectry. 48 (1980) 393.
[54] W. Jarzeba, G.C. Walker, A.E. Johnson, M.A. Kahlow and P.F. Barabara, J. Phys. Chem. 92 (1988) 7039.
[55] V.L. Bogdanov and V.P. Klochkov, Opt. Spectry. 44 (1978) 412; 45 (1978) 51; 52 (1982) 41.
[56] M.J. Rosker, F.W. Wise and C.L. Tang, Phys. Rev. Letters 57 (1986) 321;
F.W. Wise, M.J. Rosker and C.L. Tang, Phys. Rev. Letters 86 (1987) 2827.
[57] B.D. Fainberg, Opt. Spectry. 65 (1988) 722.

[58] F. Wondrazek, A. Seilmeier and W. Kaiser, Chem. Phys. Letters 104 (1984) 121.
[59] S.H. Lin, Theoret. Chim. Acta 10 (1968) 301.
[60] B.D. Fainberg, Opt. Spectry. 49 (1980) 95.
[61] B.D. Fainberg, Opt. Spektroskopiya 63 (1987) 738 [Opt. Spectry. 63 (1987) 436].
[62] Y.J. Yan and S. Mukamel, J. Chem. Phys. 89 (1988) 5160.
[63] Y.J. Yan and S. Mukamel, Phys. Rev. A 41 (1990) 6485.
[64] B.D. Fainberg, Israel J. Chem. 33 (1993) 25.
[65] S.K. Garg and C.P. Smyth, J. Phys. Chem. 69 (1965) 1294.
[66] D. Bertolini, M. Casettari and G. Salvetti, J. Chem. Phys. 78 (1983) 365.
[67] A.El. Samahy, B. Gastblom and J. Sjoblom, Finn. Chem. Letters (1984) 54.
[68] B.P. Jordan, R.J. Sheppard and S.J. Szwarnowski, J. Phys. D 11 (1978) 695.
[69] G.E. McDuffie Jr., R.G. Quinn and T.A. Litovitz, J. Chem. Phys. 37 (1962) 239.
[70] M.W. Sagal, J. Chem. Phys. 36 (1962) 2437.
[71] Landolt–Börnstein, Zahlenwerte und Funktionen aus Physik, Chemie, Astronomie, Geophysik und Technik, Vol. 2, Part 5a (Springer, Berlin, 1969);
C.J.F. Böttcher and P. Bordewijk, Theory of electric polarization. Vol. 2 (Elsevier, Amsterdam, 1978) chs. 7, 9.
[72] G.J. Blanchard, J. Chem. Phys. 95 (1991) 6317.
[73] H. Mori, Rept. Prog. Phys. 33 (1965) 423;
R. Kubo, Rept. Prog. Phys. 29 (1966) 255;
S.A. Adelman and J.D. Doll, J. Chem. Phys. 64 (1976) 2375.
[74] M.A. Kahlow, W. Jarzeba, T.J. King and P.F. Barbara, J. Chem. Phys. 90 (1989) 151.